Midlatitude daytime D region ionosphere variations measured from radio atmospherics

Feng Han[1] and Steven A. Cummer[1]

Received 25 May 2010; revised 15 July 2010; accepted 28 July 2010; published 14 October 2010.

[1] We measured the midlatitude daytime ionospheric D region electron density profile height variations in July and August 2005 near Duke University by using radio atmospherics (or sferics for short), which are the high-power, broadband very low frequency (VLF) signals launched by lightning discharges. As expected, the measured daytime D region electron density profile heights showed temporal variations quantitatively correlated with solar zenith angle changes. In the midlatitude geographical regions near Duke University, the observed quiet time heights decreased from ~80 km near sunrise to ~71 km near noon when the solar zenith angle was minimum. The measured height quantitative dependence on the solar zenith angle was slightly different from the low-latitude measurement given in a previous work. We also observed unexpected spatial variations not linked to the solar zenith angle on some days, with 15% of days exhibiting regional differences larger than 0.5 km. In these 2 months, 14 days had sudden height drops caused by solar flare X-rays, with a minimum height of 63.4 km observed. The induced height change during a solar flare event was approximately proportional to the logarithm of the X-ray flux. In the long waveband (wavelength, 1–8 Å), an increase in flux by a factor of 10 resulted in 6.3 km decrease of the height at the flux peak time, nearly a perfect agreement with the previous measurement. During the rising and decaying phases of the solar flare, the height changes correlated more consistently with the short, rather than the long, wavelength X-ray flux changes.

Citation: Han, F., and S. A. Cummer (2010), Midlatitude daytime D region ionosphere variations measured from radio atmospherics, *J. Geophys. Res.*, *115*, A10314, doi:10.1029/2010JA015715.

1. Introduction

[2] The ionospheric D region electron density profiles can be probed using very low frequency (VLF) electromagnetic waves (3–30 kHz) that are reflected by the lower ionosphere. Previous work along these lines has mainly focused on the measurements of D region electron density profiles using single frequency or narrowband signals. *Deeks* [1966] presented the height of D region electron concentration over England and discussed its variations with the time, year and sunspot cycle as well as eclipse effects through using 16 kHz experiment data. *Thomson* [1993] reported the daytime two parameter exponential D region electron density profile as well as its solar zenith angle dependence by comparing the amplitudes and phases of simulated signals to measured quantities for long paths averaging from different VLF transmitters. *McRae and Thomson* [2000] studied the dependence on solar zenith angles of experimentally observed daytime variations of VLF phases and amplitudes over a variety of long subionospheric paths, as well as the dependence on solar zenith angles of inferred D region electron density profiles.

[3] Daytime VLF remote sensing has also been used to measure ionosphere perturbations caused by solar flare X-rays. The major ionization source of the undisturbed ionospheric D region from which the VLF signals are reflected is the Lyman-α ultraviolet from solar radiation. When a solar flare (X-ray) occurs, the X-ray fluxes increase suddenly and those with wavelength appreciably below 1 nm are able to penetrate down to D region and increase the ionization rate there [*Thomson and Clilverd*, 2001]. A lot of work has been done regarding the correlation between X-ray fluxes and VLF perturbations as well as D region electron density profiles. *Pant* [1993] showed that the VLF phase deviation increased linearly with the logarithm increase of X-ray fluxes by comparing the solar flare X-ray flux data between 1977 and 1983 to the measured VLF phase shifts. *McRae and Thomson* [2004] studied VLF amplitude and phase perturbations during several solar flare events, and quantitatively correlated the two parameter exponential D region electron density profile changes with X-ray fluxes when they achieved their peak values. *Thomson et al.* [2004, 2005] deduced X-ray fluxes for several big solar flares including the one on 4 November 2003 from VLF phase shifts during solar flare periods. Most

[1]Department of Electrical and Computer Engineering, Duke University, Durham, North Carolina, USA.

Copyright 2010 by the American Geophysical Union.
0148-0227/10/2010JA015715

of these studies focused on relating the maximum X-ray flux and the maximum D region change during the period of a solar flare event.

[4] Compared to the narrowband VLF signals which only provide measurements of the amplitude and phase, the broadband VLF sferic signals discharged by lightning strokes include rich information in a broad frequency range, and can be used to remote sense the ionospheric D region electron density profile variations. *Cummer et al.* [1998] inferred the average D region electron density profiles across the sferic wave propagation paths by comparing the measured and model simulated sferic characteristics. *Smith et al.* [2004] derived D region reflection height variations over a 24 h period from VLF/LF electric fields which were discharged by intracloud lightning and recorded by the Los Alamos Sferic Array (LASA). *Cheng et al.* [2006] measured D region electron density profile variations of 16 nights in 2004 by fitting the Long Wave Propagation Capability (LWPC) modeled spectra to measured sferic spectra. *Jacobson et al.* [2007] retrieved the D region reflection height variations with time, geographical locations, solar radiation and X-ray fluxes based on 3 year Narrow Bipolar Events (NBE). *Jacobson et al.* [2010] proposed the broadband, single-hop method to derive the two-parameter exponential D region electron density profile, and pointed out that this method can be potentially used to study localized and transient disturbances. However, the D region electron density temporal variations in time scales from minutes to hours were not reflected in those measurements.

[5] In a recent paper [*Han and Cummer*, 2010], we calculated the nighttime D region equivalent exponential electron density profile height variations over two months by fitting a series of finite difference time domain (FDTD) model [*Hu and Cummer*, 2006] simulated sferic spectra to the measured sferic spectrum in the VLF lower frequency band (3–8 kHz). We presented the statistical results of hourly averaged heights and temporal variations on time scales from minutes to hours as well lateral spatial gradients of the measured D region.

[6] In this work, we used similar data and methods to calculate the midlatitude daytime ionospheric D region electron density profile height variations in July and August 2005 near Duke University. A total of 285,029 National Lightning Detection Network (NLDN) recorded lightning strokes was used to almost continuously monitor the D region variations on daytime between 06 and 20 local time (LT). The local time we used in this work is the same as Eastern Daylight Time (EDT) which is 4 h behind Universal Time (UT). This means the solar zenith angle is not the minimum at 12 LT. The variations of D region electron density profile heights in time scales of minutes to hours were calculated. Instantaneous measurements of geographical variations beyond the solar zenith angle effects were studied by comparing the measured effective heights in two different regions. The solar zenith angle dependence of measured heights slightly differs from previous results from single frequency measurements [*Ferguson*,1980; *McRae and Thomson*, 2000], but is restricted to small midlatitude regions, rather than long paths spatially averaged. We correlated X-ray fluxes with measured heights in X-ray rising phases, peaks and decaying phases, and found that the logarithm of the flux is approximately proportional to the measured height change. However, the solar flare has stronger effects on the D region in the X-ray rising phase than in the decaying phase.

2. Data Analysis Method

2.1. Description of Experimental Data

[7] Lightning data having time resolution less than one millisecond and location resolution less than 500 m are provided by NLDN, which detects cloud-to-ground (CG) lightning flashes with the peak current larger than 5 kA, and with an efficiency ranging from 80% to 90% [*Cummins et al.*, 1998]. The sferic data are recorded by the broadband VLF/ELF receivers located near Duke University [*Cheng*, 2006]. Although both azimuthal (B_ϕ) and radial (B_r) components of the horizontal magnetic fields can be calculated from the measured signals, we only use B_ϕ in order to avoid low signal to noise ratio (SNR), and thus increase the reliability of measured results [*Cummer et al.*, 1998; *Cheng et al.*, 2006; *Han and Cummer*, 2010].

[8] Figure 1 shows seven typical measured daytime B_ϕ spectra excited by NLDN recorded lightning strokes. Figure 1a shows the general shape of a typical daytime sferic spectrum. Different from the nighttime B_ϕ which contains the fine frequency structures caused by the Earth-ionosphere waveguide mode interference in 3–8 kHz [*Han and Cummer*, 2010], those frequency structures of daytime B_ϕ appear in the 1.5–4 kHz band. The spectrum in ≥4 kHz frequency range is typically smooth for a daytime sferic. It is from these fine frequency structures in 1.5–4 kHz range that the daytime D region electron density profile heights are extracted.

[9] Three sferic spectra in Figure 1b which were generated by lightning strokes 650 km from the east coast of the United States in the morning on 1 July 2005 show a 2 h period between 0710 LT and 0917 LT that exhibits significant frequency changes, and thus ionosphere variations over that time. Three sferic spectra in Figure 1c which were generated by lightning strokes around 550 km west of Duke sensors during the noontime on 1 July 2005 show a 1 h period between 1316 LT and 1419 LT in which the ionosphere was relatively stable. Although the spectral magnitudes are slightly different between 1.5 and 4 kHz, the fine frequency structure (peaks and valleys) positions which are closely related to the ionosphere state are almost the same.

[10] We only analyze here the sferic data in July and August 2005 since the data acquisition system was operated in the continuous mode in these 2 months, meaning all sferics were recorded. Only daytime data between 06 and 20 LT (10–24 UT, approximately between sunrise and sunset near Duke University) were used. In addition, only lightning strokes that occurred between 500 and 800 km away were used to minimize spatial averaging of any ionosphere variation and that the signals exhibit clear mode interference patterns in 1.5–4 kHz [*Han and Cummer*, 2010]. A criterion of 30 kA threshold was applied to the lightning peak current selection to ensure that each sferic has a favorable SNR.

2.2. Model Simulations of VLF Sferic Propagation

[11] The heights of D region electron density profile are derived by comparing the measured sferic spectra to the FDTD simulation results. In the simulations, we use the

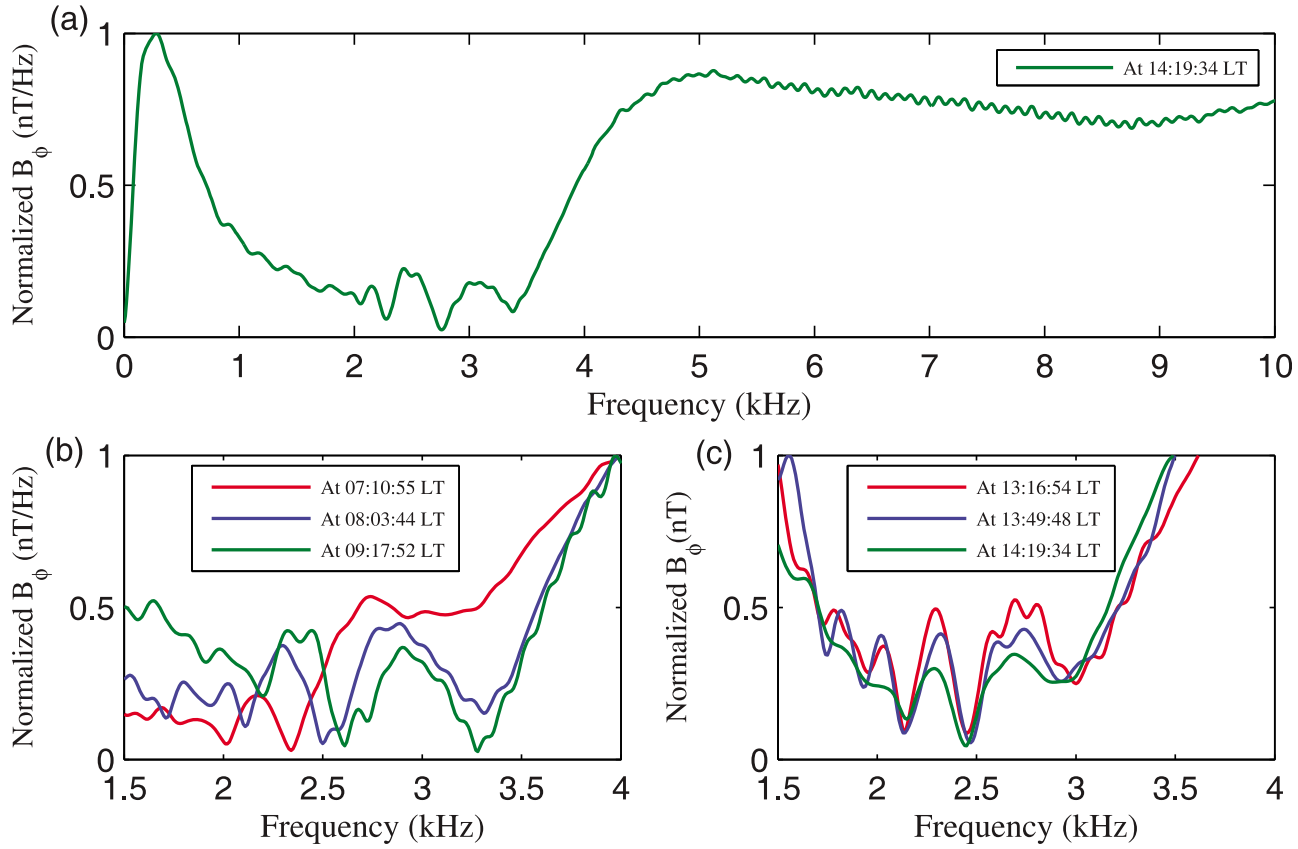

Figure 1. Daytime sferic spectra for lightning at different time but from almost the same location. (a) The general shape of the daytime sferic spectrum; fine structures in ≥4 kHz range disappear. (b) Events in the morning of 1 July 2005 demonstrates the strong variation with time of the daytime D region. (c) Events during noontime of 1 July 2005 show little variation.

standard D region electron density profile parameterizations of

$$N_e(h) = 1.43 \times 10^7 \exp(-0.15h') \times \exp[(\beta - 0.15)(h - h')]\text{cm}^{-3} \quad (1)$$

with h' in km and β in km^{-1} [*Wait and Spies*, 1964]. This functional form is an equivalent exponential profile that may be different from the more complex true profiles [*Smith and Klaus*, 1978; *Goldberg et al.*, 1997]. However, *Cheng et al.* [2006] showed this equivalent profile can reproduce the major sferic propagation effects compared to rocket measured electron density profiles [*Mechtly and Smith*, 1968; *Smith and Gilchrist*, 1984]. It has been successfully used in VLF measurements [*Cummer et al.*, 1998; *McRae and Thomson*, 2000; *Cheng et al.*, 2006; *Thomson et al.*, 2007; *Thomson and McRae*, 2009; *Han and Cummer*, 2010]. The parameter h' controls the height of the electron density profile while β controls the sharpness of the profile. The ion density profiles (including positive and negative ions) are not well constrained in measurements. We performed FDTD model simulations and found that an increase in the ion densities by a factor of 10 has a negligible effect on waveguide mode interference patterns from which the equivalent exponential profile height is extracted. Therefore, the classical ion density profiles [*Narcisi*, 1971; *Cummer et al.*, 1998; *Han and Cummer*, 2010] are used in this work. There are also uncertainties in the D region collision frequency profiles (including electron collision frequency profiles, positive ion collision frequency profiles and negative ion collision frequency profiles) [*Phelps and Pack*, 1959; *Thrane and Piggott*, 1966; *Friedrich and Torkar*, 1983]. We performed FDTD model simulations and found that change from the profile adapted from *Thrane and Piggott* [1966] to the profile from *Wait and Spies* [1964], around an increase in the frequencies by a factor of 10, can shift the sferic spectrum, which is equal to a shift caused by 0.6 km h' change. It means an error of 0.6 km of the measured h' is caused by an uncertainty of 10 times of the collision frequencies. In order to compare the measured h' to the results given by *McRae and Thomson* [2000, 2004], we use the profiles [*Wait and Spies*, 1964; *Morfitt and Shellman*, 1976; *Cummer et al.*, 1998; *Han and Cummer*, 2010] which are widely used in VLF literature. Although the true ion density profiles and collision frequency profiles can be different from the profiles we used in this work, the insensitivity of the waveguide mode interference pattern of a spectrum on ion densities and collision frequencies means the derived equivalent exponential profile height is precise and reliable.

[12] Earth's background magnetic field is important. FDTD model simulations showed that lowering one order of the total magnetic field decreases the magnitude of the

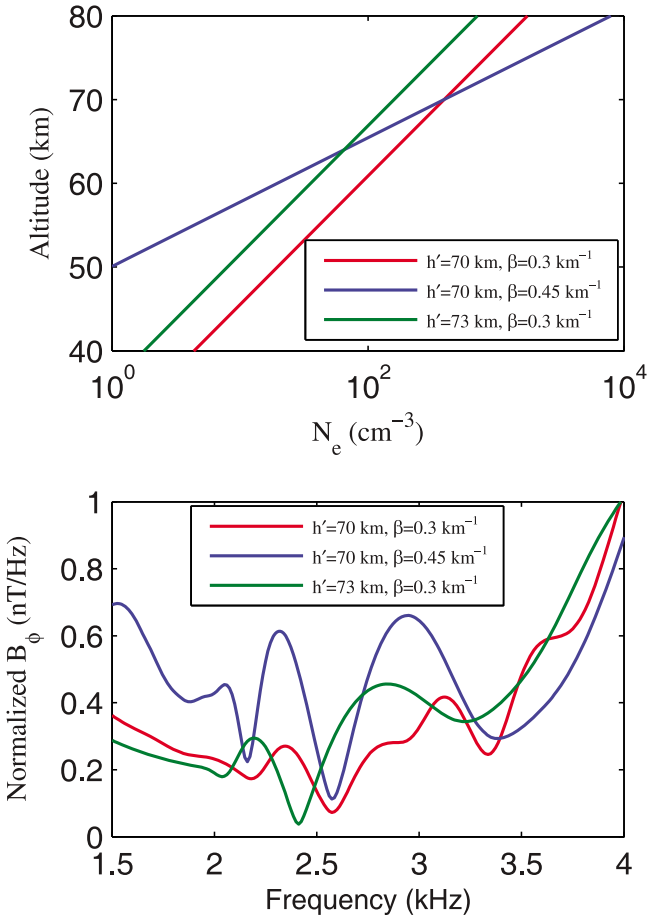

Figure 2. Three typical daytime D region electron density profiles and the corresponding simulated sferic spectra under those profiles. (top) Electron density profiles. (bottom) Sferic spectra. The lower VLF signal spectrum is very sensitive to h' but much less sensitive to β.

waveguide mode interference pattern to one fifth of its original value due to the attenuation of the Transverse Magnetic (TM) modes in the Earth-ionosphere waveguide. The weaker waveguide mode interference pattern makes the positions of those peaks and valleys in the mode interference pattern more difficult to locate. Because the simulated sferic wave propagation is in the midlatitude and the size of simulation domain is much smaller than Earth radius, the vector magnetic field is treated as homogenous in the whole simulation domain with the magnitude 5×10^4 nT and dip angle 65°. The azimuth dependence of the wave propagation is also included. It means the geomagnetic field is uniform in the simulation domain but is domain relative to wave propagation. It varies to reflect the real propagation geometry [*Hu and Cummer*, 2006].

[13] The upper boundary of the simulation domain is modeled by the two-parameter electron density profile described by (1). The lower boundary, the ground, is treated as a Perfect Electrical Conductor (PEC) in previous work [*Ma et al.*, 1998; *Cummer*, 2000; *Han and Cummer*, 2010]. Since the measurement of D region electron density profiles in this work mainly depends on the lower-frequency range (below 4 kHz), the PEC approximation will not affect the results because the true ground can be treated as a PEC for lower-frequency signals [*Balanis*, 1989; *Han and Cummer*, 2010]. Perfect Matched Layers (PML) are used to absorb outward propagating sferic waves so as to avoid artificial reflections [*Hu and Cummer*, 2006]. The source lightning return stroke in FDTD simulations is modeled by *Jones* [1970] and *Dennis and Pierce* [1967] which was used by *Cheng et al.* [2006] and *Han and Cummer* [2010]. In the analysis below, the source spectrum is normalized out, and the source waveform does not influence the results. Some lightning source spectra are not flat and cannot be completely normalized out. However, they do not affect the major variation trend of the measured h' because they are rather uncommon.

2.3. Influence of D Region Parameters on VLF Spectra

[14] The parameters h' and β have similar effects on a daytime sferic spectrum as on a nighttime sferic spectrum [*Han and Cummer*, 2010], and this is illustrated in Figure 2. The top frame shows three sample daytime electron density profiles and the bottom frame shows the corresponding simulated sferic spectra for those profiles. The waveguide mode interference fringes are altered by h' variation in the same way as they are at night, i.e., a larger h' causes the waveguide mode interference fringes to shift to lower frequency bands. It is from these fringe positions that h' is extracted. In contrast, a change in β affects the magnitudes of these fringes but very minimally changes their positions. FDTD model simulations showed that increasing β from 0.3 to 0.45 km^{-1} leads to the measured h' change of less than 0.1 km. These magnitude changes cannot be directly used to infer β because variations in received signals are perhaps due to differences in lightning current waveforms and channel orientations.

[15] Consequently, in this work, we only report measurements of h' variations. *McRae and Thomson* [2000] found that, at solar minimum, β varied from ~0.24 km^{-1} near dawn/dusk to ~0.4 km^{-1} around midday. We assume an average daytime value of $\beta = 0.3$ km^{-1}. Although we only measured h', the results are reliable and quantitatively meaningful because the method we used is insensitive to β changes. The fine frequency structure of a daytime sferic spectrum is sensitive to propagation distances but insensitive to azimuth angles, i.e., a larger distance shifts the fine frequency structures up in frequency, whereas a change of 30 degrees of the azimuth angle has little effect on them. This is also true for a nighttime sferic spectrum [*Han and Cummer*, 2010].

2.4. Profile Height Measurement

[16] Similar to the procedure for nighttime measurements [*Han and Cummer*, 2010], we extracted the parameter h' from a measured daytime sferic spectrum by comparing it to a series of simulated sferic spectra from the FDTD model simulations under different electron density profiles. A simulated sferic database was set up for lightning strokes from different distances and azimuth angles. Propagation distances vary with step 20 km; azimuth angles vary from 0 to 360 degrees with step 30 degrees; electron density profiles were modeled, with h' varying from 60 to 80 km with step 0.2 km, and β fixed to be 0.3 km^{-1}. An automatic fitting algorithm was constructed to find the best fitted

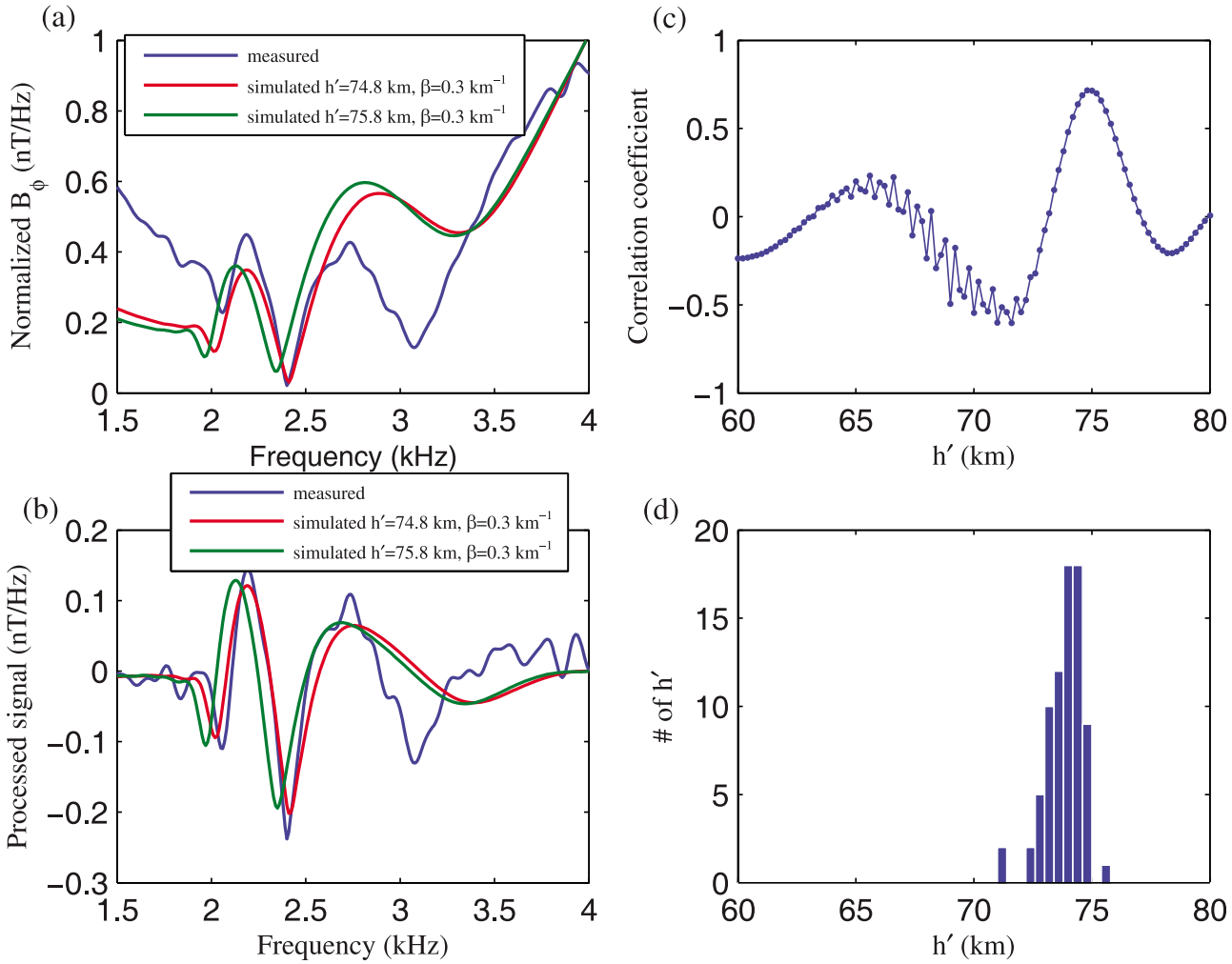

Figure 3. The sferic spectrum fitting procedure: (a) fitting for the original spectrum, (b) fitting for the peaks and valleys caused by waveguide interference, (c) correlation coefficients between the measured and simulated processed signals for different h' values, and (d) the histogram of individual h' in a 5 min window. The standard deviation is 0.77 km.

simulated sferic spectrum for each recorded sferic excited by a lightning stroke in a certain azimuth and distance, i.e., to derive the electron density profile parameter h' for β = 0.3 km^{-1} across the wave propagation path.

[17] The h' value is derived in following four steps. At first, the program fetches from the database the simulated sferics that have the azimuth angle and two distances nearest to the azimuth angle and distance of the measured sferic. Then, the program code selects several simulated sferic spectra, with an appropriate range of h', whose middle valleys align with one valley of the measured sferic spectrum in 1.5–4 kHz frequency range. Usually, the daytime sferic spectrum has three obvious valleys in 1.5–4 kHz frequency range and the valley that has the smallest amplitude is the middle one. As shown in Figure 3a, the middle valleys are at around 2.5 kHz and have the smallest amplitude values for both measured and simulated sferic spectra. However, for some simulations, the amplitudes of the middle valleys can be slightly larger than the amplitudes of valleys in their left or right. Therefore, before running the code, the middle valley positions for all the simulated sferic spectra are saved in a lookup table. Although the amplitudes of the middle valleys are the smallest for some sferics but not for others, they can be located precisely according to their shift with h' and distance variations. The selected simulated sferic spectra whose middle valleys align with one valley of the measured sferic spectrum in 1.5–4 kHz frequency range are termed "first batch sferics." The "second batch sferics" are generated by adding other sferics corresponding to h' 0.2 km smaller and 0.2 km larger than the h' for each of the "first batch sferics" to them [*Han and Cummer*, 2010].

[18] In the second step, the fine frequency structures caused by waveguide mode interference in frequency range 1.5–4 kHz are extracted from both the "second batch sferics" spectra and the measured sferic spectrum using the same method as for nighttime sferic fitting [*Han and Cummer*, 2010]. However, the correlation coefficients are calculated between 1.5 kHz and 4 kHz since most daytime sferic spectra information is contained in this frequency range. The "third batch sferics" are generated by selecting

three fitted sferic spectra corresponding to the three largest correlation coefficients.

[19] Figures 3a and 3b show this procedure. The sferic spectra fitting between the measured and the simulated is more obviously shown by the processed signal in b, which is actually the fine frequency structures caused by mode interference, than by original spectra in a. It is clear the spectra fitting for h' = 74.8 km is better than that for h' = 75.8 km due to the position alignments of those fine frequency structures. The "third batch sferics" corresponding to h' = 74.6, 74.8 and 75 km have the largest correlation coefficients. The algorithms in the third step and the fourth step are the same as in the nighttime sferic fitting procedure [*Han and Cummer*, 2010].

[20] Figure 3c shows the typical correlation coefficients between the measured and simulated processed signals for different h' values. The h' = 74.8 km corresponds to the largest correlation coefficient and is thus usually the "measured" value. For this single sferic measurement, the correlation coefficient drops to approximately 60% of the maximum value at ±0.8 km from the best value. This indicates a typical uncertainty of ±0.8 km in h' from a single sferic.

[21] Figure 3d shows a histogram of the measured h' from 77 sferics in a 5 min time window for lightning strokes from almost the same location on 3 July 2005. The D region h' was stable during that 5 min. The measured h' had a mean value of 73.8 km and standard deviation of 0.77 km. This 0.77 km standard deviation matches the ±0.8 km uncertainty we expect for a single measurement. Thus, by averaging many single measurements in a 5 min time window, we can significantly reduce the measurement uncertainty. We chose a 5 min window for averaging as this typically provides at least several tens of sferics, and thus the uncertainty reductions of 5 to 10, and precision of 0.1 km or better.

[22] We use the maximum correlation coefficient acquired in the second step to judge the reliability of the measured h'. We only keep the single sferic measurement with the maximum correlation coefficient larger than 0.5 to ensure the reliability of the single measurement in the averaging procedure.

3. Statistical Results

[23] We applied the algorithm discussed in the last section to 285,029 lightning strokes that occurred during the daytime between 06 LT and 20 LT, and 500–800 km from the Duke sensors in July and August 2005, with solar zenith angle range 10–90 degrees. Since in the FDTD model the ground altitude is treated as constant for all simulations, the true h' values corresponding to the sea level were calculated by adding the average real ground altitude (ranging from 0 to ~500 m near Duke University) along the wave propagation path to the h' values derived from the spectra fittings. All the h' measurements shown in following sections are referenced to the sea level.

3.1. Daytime Temporal Variations

[24] The daytime D region shows variations on time scales less than 1 h due to solar radiation and other sources such as solar X-ray flares. To illustrate the detailed measured h' variation with time, we present two examples of daytime h' measurements. In both cases, there are several hundreds of individual measured sferics from which we calculate the high precision 5 min average h' values. Some individual h' measurements are far from the 5 min average values because some irregular sferic spectra caused by noise or unusual source lightning waveforms are not correctly distinguished by the h' derivation program code. This will not affect the 5 min average value calculation due to the very limited number of those "outlier" measurements.

[25] The first example is for h' measurement between 0615 and 2000 LT on 1 July 2005. Figure 4 (top) shows the h' variation extracted from 5967 sferics excited by NLDN recorded lightning strokes from the east, northeast and southwest of Duke sensors and in a range of 500–800 km from the sensors. The solar zenith angles are slightly different for measured h' in different geographical regions and their correlation will be discussed in next section. The D region electron density profile height began to drop at 0640 LT from 80.0 km and reached the lowest point 71.3 km at 1330 LT. Then, the measured height gradually increased to 77.2 km at 20 LT. The lack of measurements between 1810 LT and 1840 LT was due to missing data.

[26] The D region height variation on 1 August 2005 exhibits different features and is shown in Figure 4 (bottom), base on 5521 sferics originating to the south of the Duke sensors in a range of 500–700 km. The general variation trend of the measured h' is similar to that on 1 July 2005, i.e., the h' began to decrease from 80.0 km from the sunrise and reached 71.4 km at 1240 LT and began to increase again. However, there were two h' sudden drops caused by solar flare X-ray in the measurement period. The first one began at 0815 LT and the h' decreased to 72.2 km 10 min later and recovered to 74.2 km at 0855 LT. The second sudden drop began at 0915 LT but finished at 11 LT, and the minimum measured h' 68.0 km appeared at 0950 LT.

[27] These two examples show two types of daytime h' variations observed. If the sudden drops are not considered, the h' always drops from sunrise to noontime and then increases again until the sunset. Measured h' variations without sudden drops were observed on 48 days. Nine days showed only one sudden drop while 5 days showed more than one sudden drop. Three days had h' drops lower than 65 km with the lowest value 63.4 km observed on 13 July 2005. All of the observed sudden drops were associated with X-ray flares.

3.2. Dependence of h' on Solar Zenith Angle

[28] The D region electron density profile height variation shows close relationship with solar zenith angle changes, and this was quantitatively analyzed in literature [*Thomson*, 1993; *McRae and Thomson*, 2000; *Jacobson et al.*, 2007]. In order to illustrate this, we compared the measured h' to solar zenith angles at the midpoints of the propagation paths between Duke sensors and lightning stroke locations. Figure 5 (top) shows the dependence of the measured h' variation on solar zenith angles extracted from 5657 NLDN recorded lightning strokes over the ocean to the east of the sensors and in a range of 500–800 km from the sensors. In order to distinguish the periods before noontime and after noontime, we label the morning solar zenith angle as negative values [*McRae and Thomson*, 2000]. From sunrise to noontime, the local solar zenith angle decreased

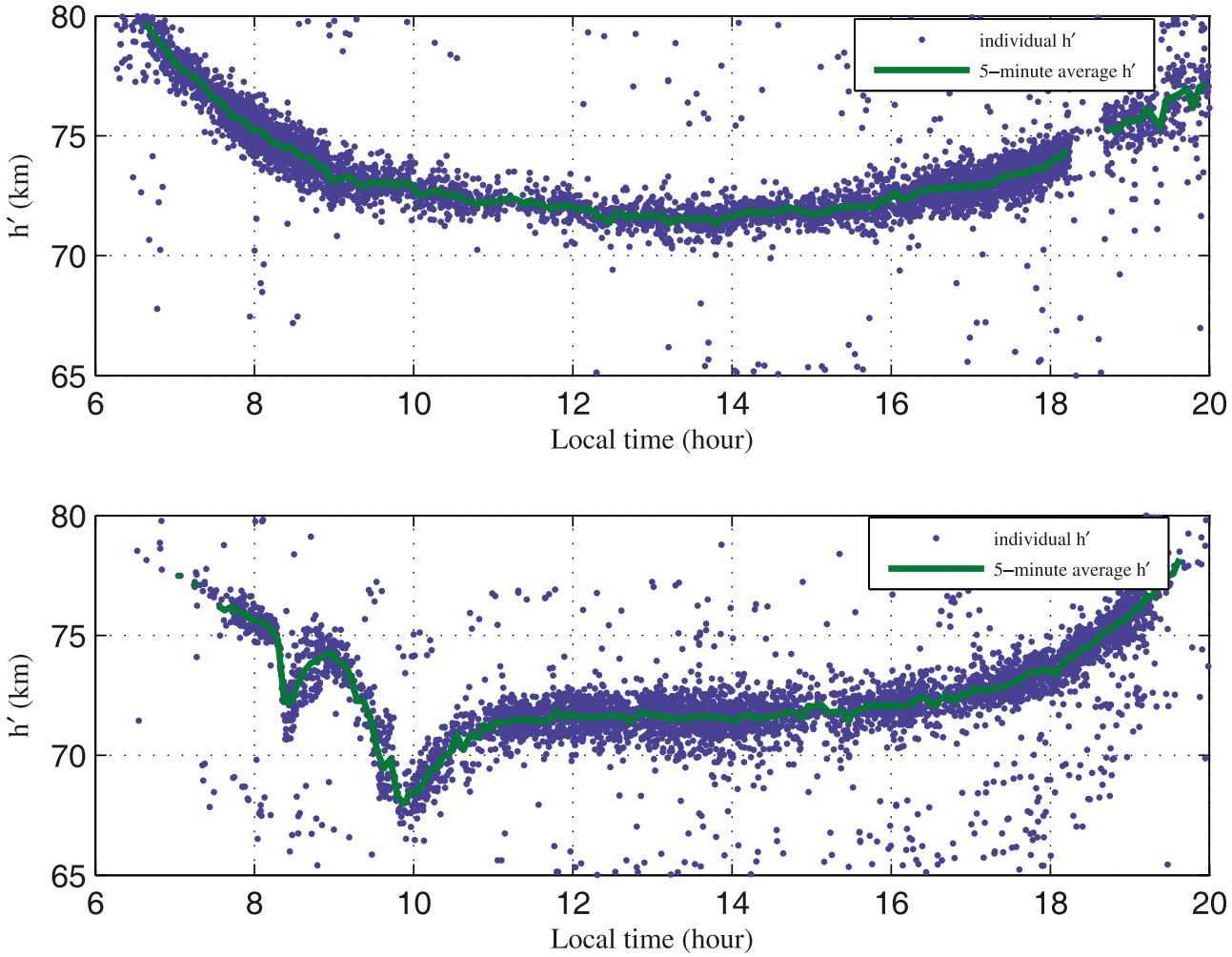

Figure 4. Typical measured h' distributions for 2 days. (top) h' variations on 1 July 2005, a typical day without solar flare X-ray disturbances. (bottom) h' variations on 1 August 2005, a typical day with obvious solar flare X-ray disturbances.

from 90 degrees to 17 degrees at 1305 LT, and during the same period, the measured h' decreased from 79.0 km to 71.5 km. The solar zenith angle began to increase and reached 87 degrees at 20 LT when the measured h' increased to 78.5 km. The minimum measured h' 71.5 km on that day appeared when the solar zenith angle was 17 degrees, which was slightly higher than the value 70.8 km given by *McRae and Thomson* [2000] for the same solar zenith angle 17 degrees in near solar minimum years (1994–1997). This is not surprising given that our measurements were restricted to a small geographical region in the mid-latitude in a near solar minimum year, while *McRae and Thomson* [2000] used the single frequency VLF signals propagating across the equator to measure h' in lower latitudes. In addition, the measured h' changed quickly when the solar zenith angle was larger than ~50 degrees, which is consistent with the statistical results given by *Jacobson et al.* [2007].

[29] In order to quantitatively correlate the derived h' variations with solar zenith angle changes, we calculated the statistical results of the measured h' and solar zenith angle in July and August 2005. In each 5 min time window, the locations of source lightning strokes are grided into 2° × 2° geographical regions. Such a region is large enough to include several tens to hundreds of lightning strokes but small enough to minimize the spatial variation. The mean values of the measured h' and solar zenith angles in the middle points across the sferic wave propagation paths were calculated for each 2° × 2° geographical region and each 5 min time window that has more than 20 NLDN recorded lightning strokes, so as to ensure the reliability of the statistical result. The measured h' sudden drops caused by solar flare X-rays are not included in this result since they have no direct relationship with solar zenith angle changes. We did not distinguish the h' dependence on solar zenith angle before and after noontime since calculations showed they are the same. Figure 5 (bottom) shows our result compared to results from other models.

[30] We compared our measured result to the polynomial calculation given by *McRae and Thomson* [2000] for near solar minimum years. Our measured h' values are higher than the heights calculated from the polynomial model, especially when the solar zenith angle is smaller than 70 degrees. This is possibly due to different measured regions,

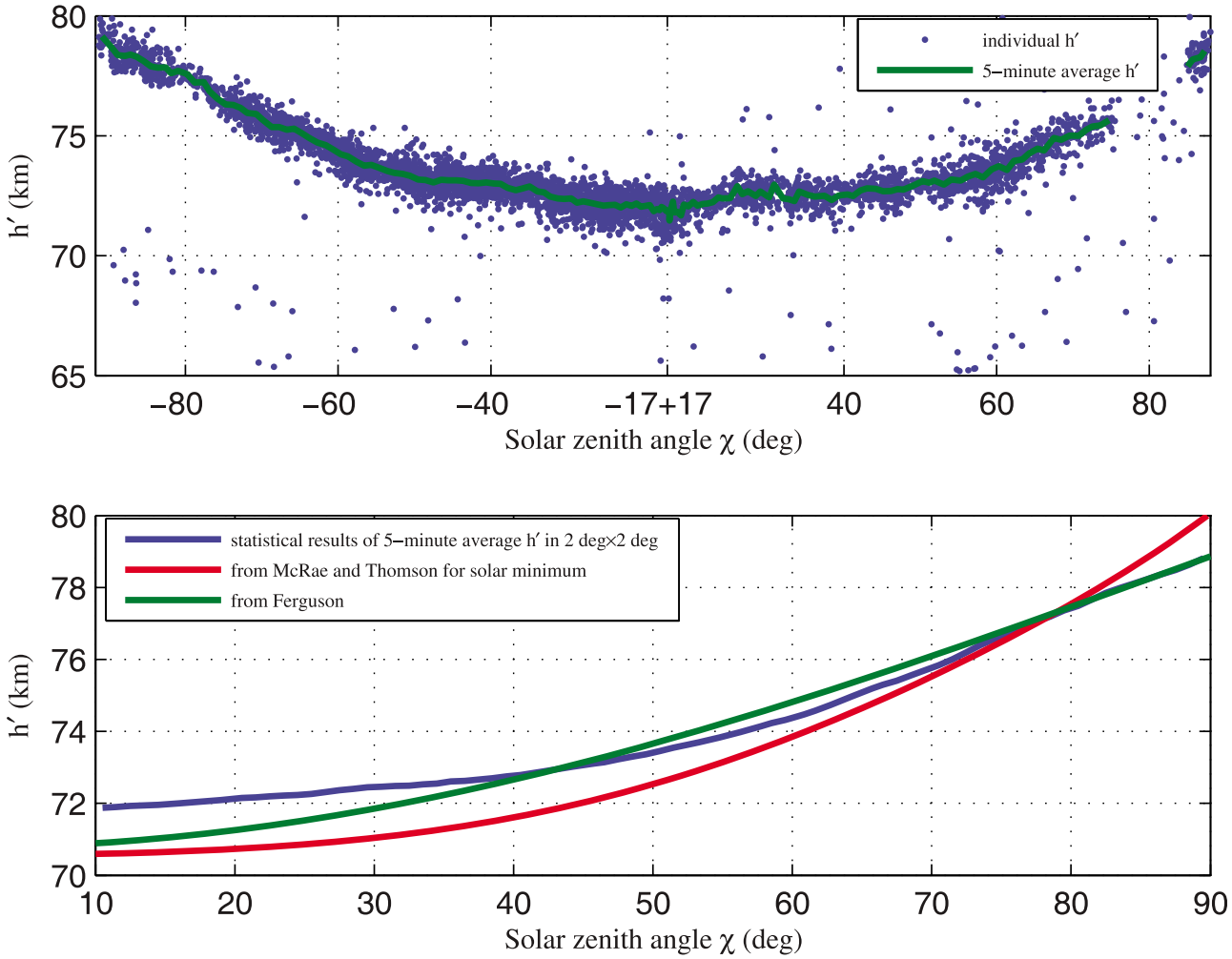

Figure 5. The measured h' dependence on solar zenith angle. (top) The measured h' and solar zenith angle variation on 22 July 2005; the measured h' when the solar zenith angle minimum was slightly higher than the result given by *McRae and Thomson* [2000]. (bottom) The statistical result on 2 months compared to calculations from *McRae and Thomson* [2000] and *Ferguson* [1980]; the general variation trends are similar, while the specific values are different for the same solar zenith angle. The solar zenith angle near Duke University was bounded between 10° and 90° during the 2 months, although the minimum solar zenith angle on 22 July 2005 was 17°.

i.e., our measurements were in small midlatitude regions while *McRae and Thomson* [2000] measured the average h' in the long paths across the equator and in low latitudes. We also compared our result to the model calculation given by *Ferguson* [1980]. Compared to the polynomial calculation given by *McRae and Thomson* [2000], this model not only include the solar zenith angle, but also the geographic location, date, sunspot number and geomagnetic activity. However, as shown in Figure 5 (bottom), only the general variation trends are similar. For the same solar zenith angles, our measured h' can also be different from the model results.

3.3. Daytime Spatial Variations

[31] Besides the variations caused by solar zenith angle changes, daytime h' measurements show unexpected spatial variations. In order to exclude the solar zenith angle influence (i.e., at the same LT, different regions have different solar zenith angles), we compared the measured h' variations for different probed regions with the same solar zenith angle instead of the same local time.

[32] Figure 6 shows two examples of simultaneous multiple D region measurements. Two groups of lightning strokes from different directions were used to measure the h' in different regions on 23 July 2005. A total of 1552 NLDN recorded lightning strokes from the southwest of Duke sensors was used to measure the h' in region 1, and 2017 strokes from the southeast of Duke sensors were used to measure the h' in region 2. Figure 6a shows the geographic distributions of lightning strokes from 15 LT to 20 LT on that day. Figure 6b shows a measured h' difference of ~0.2 km in two regions if the solar zenith angle is the same. The west region had a lower h', while ~100 km to the east, the D region was 0.2 km higher. This spatial difference was not the fluctuation in the measurement process caused by irregular source spectra or the uncertainty in the spectra minima fitting, since the 5 min averages were calculated from several

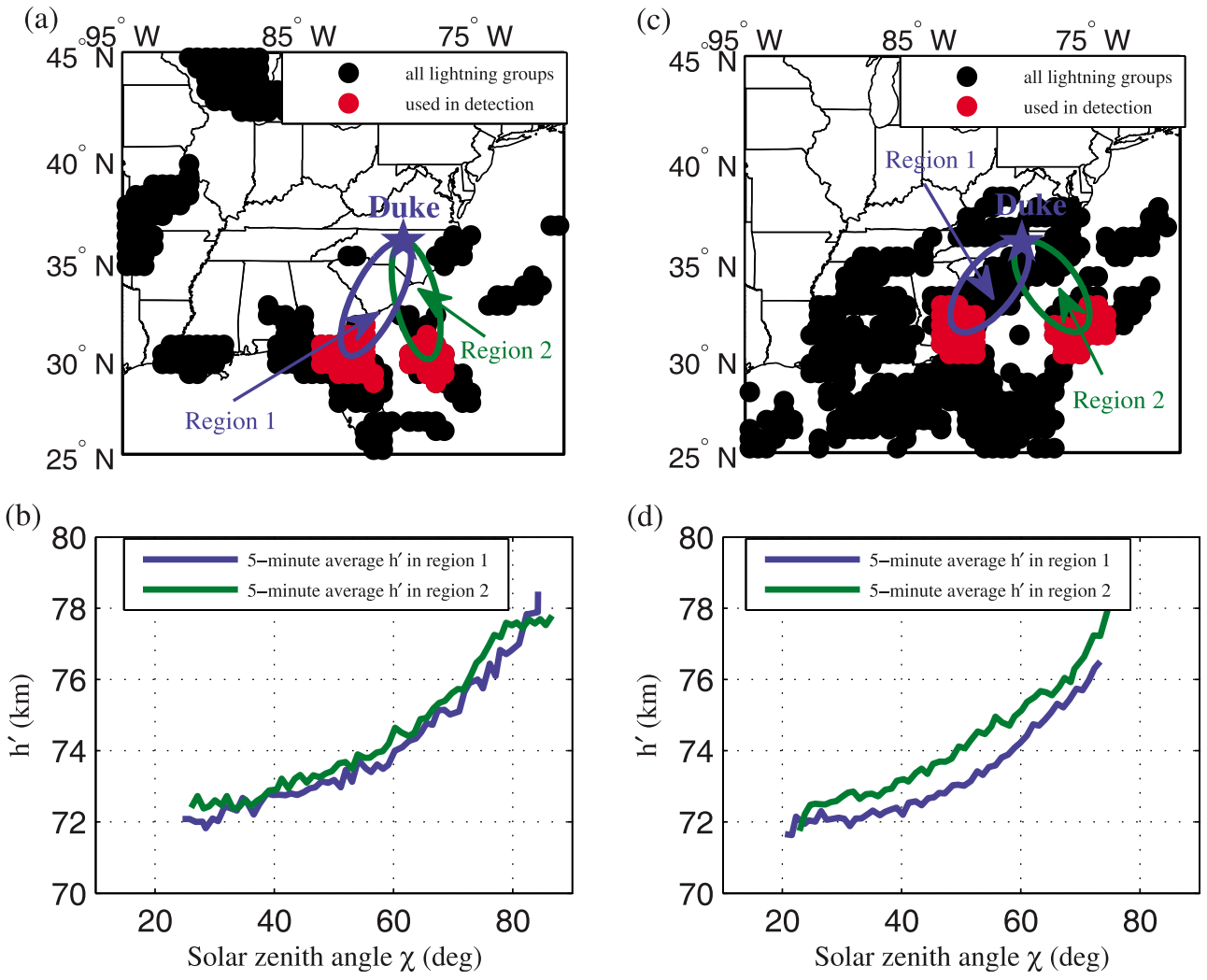

Figure 6. The h' measurements on 23 July 2005 and 30 July 2005. (a) Lightning distribution between 15 LT and 20 LT on 23 July 2005. (b) 5 min average measured h' variation between 15 LT and 20 LT on 23 July 2005. (c) Lightning distribution between 14 LT and 19 LT on 30 July 2005. (d) 5 min average measured h' variation between 14 LT and 19 LT on 30 July 2005.

tens of measurements and the uncertainty was ~0.1 km. On 30 July 2005, the spatial difference was as large as 1.0 km for the same solar zenith angles during the 5 h period from 14 LT to 19 LT, which was shown in Figures 6c and 6d. A total of 1802 NLDN recorded lightning strokes from the southwest of Duke sensors was used to measure the h' in region 1, and 2115 strokes from the southeast of Duke sensors were used to measure the h' in region 2. Similar to the previous example, the west region had a lower ionosphere height, while ~250 km to the east, it was higher.

[33] The above examples show that the daytime D region electron density profile height is dominated but not completely determined by solar radiation. The spatial variation beyond solar radiation influence exists in daytime. This spatial variation is not an artifact of propagation anisotropy since the geomagnetic azimuth effects are already included in the FDTD model and waveguide mode interference pattern fitting process. Of 61 days in 2 months, 26 days had useful lightning strokes in at least two different directions simultaneously. Eight of these days showed spatial variations of h' larger than 0.5 km for the same solar zenith angle in two different probed regions, with the maximum difference 1.0 km observed on 30 July 2005. Other days had h' difference smaller than 0.5 km, with the minimum difference 0.2 km observed on 23 July 2005.

3.4. Correlation of h' with Solar Flare X-ray Fluxes

[34] Solar flares, particularly at X-ray wavelengths, can penetrate into the ionospheric D region and change the electron density there and, thus, affect the VLF wave propagation in the Earth-ionosphere waveguide [*Mitra*, 1974]. Quantitative calculations of perturbations caused by solar flare X-ray have been performed in previous work [*Thomson et al.*, 2004; *Todoroki et al.*, 2007; *Jacobson et al.*, 2007]. In order to compare our measured h' drops to X-ray fluxes during a solar flare, we use the X-ray data recorded by the Geostationary Operational Environmental Satellite 10 (GOES-10) and provided by National Oceanic and Atmospheric Administration (NOAA). The X-ray flux was recorded in two bands: long wavelength band (X_l) with

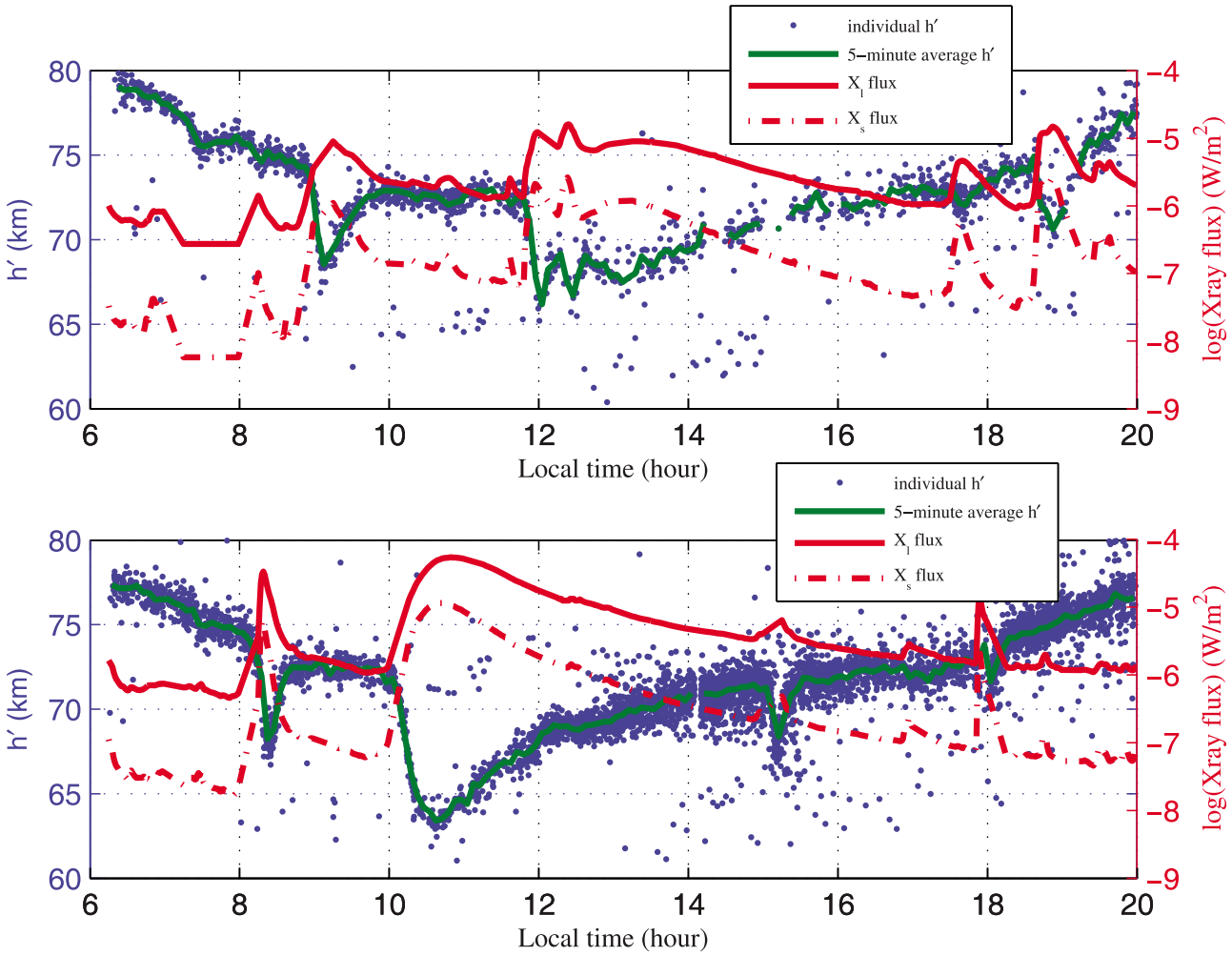

Figure 7. The measured h' related to X-ray flux variation. The measured h' sudden drops and the X-ray flux sudden increases are perfectly correlated in time. (top) On 12 July 2005. (bottom) On 13 July 2005.

wavelength 1–8 Å and short wavelength band (X_s) with wavelength 0.5–4 Å. The X_l has greater fluxes while X_s is more penetrating and so is more dominant for ionizing the bottom edge of D region, i.e., the VLF reflection height [*Mitra*, 1974; *Thomson et al.*, 2005]. In this section, we will compare both X_l and X_s fluxes to the measured h' disturbances.

[35] We first present measured h' in 2 days with significant perturbations induced by solar flare X-rays. Figure 7 (top) shows the measured h' variations with five sudden drops in nearly 14 h on 12 July 2005, by using 1663 NLDN recorded lightning strokes 500–700 km away from the Duke sensors. The measured h' sudden drops and the X-ray flux sudden increases are perfectly correlated in time. The beginning time of h' sudden drops can be defined as the time when the h' deviates from the unperturbed value corresponding to the typical height only decided by the solar zenith angle at that time. Figure 7 (bottom) shows the solar flare X-ray induced h' perturbations on 13 July 2005. The measured results were extracted from 5923 lightning strokes 500–700 km from the Duke sensors. Among the four perturbations, the one which began at 10 LT had the h' drop to 63.4 km at 1035 LT which was the lowest height in 2 months of measurements.

[36] Figure 8 shows the change of h' correlated with solar flare X-ray fluxes. Besides the correlation between peak fluxes and measured h' variations which has been studied in previous work [*McRae and Thomson*, 2004], we also studied the relationship between the measured h' and X-ray fluxes in each 5 min time window during the solar flare period. We divided the measured h' into three groups according to their measurement time in the solar flare process, i.e., they can be in the X-ray rising phase, peak and decaying phase. The $\Delta h'$ is defined as the measured h' subtracted by the unperturbed h' during the flare period. The unperturbed h' is calculated from the average value of h' in 2 months as we discussed in section 3.2. Thirteen 5 min average h' measurements during fast X-ray increases, particularly in some rising phases, are not included, since the D region may have not enough time to respond to the solar flare, and the measured h' changes are usually smaller than true changes.

[37] We compared $\Delta h'$ to the logarithm of both the long wave and short wave X-ray fluxes during the solar flare periods. Figure 8a shows the correlation between X_l fluxes

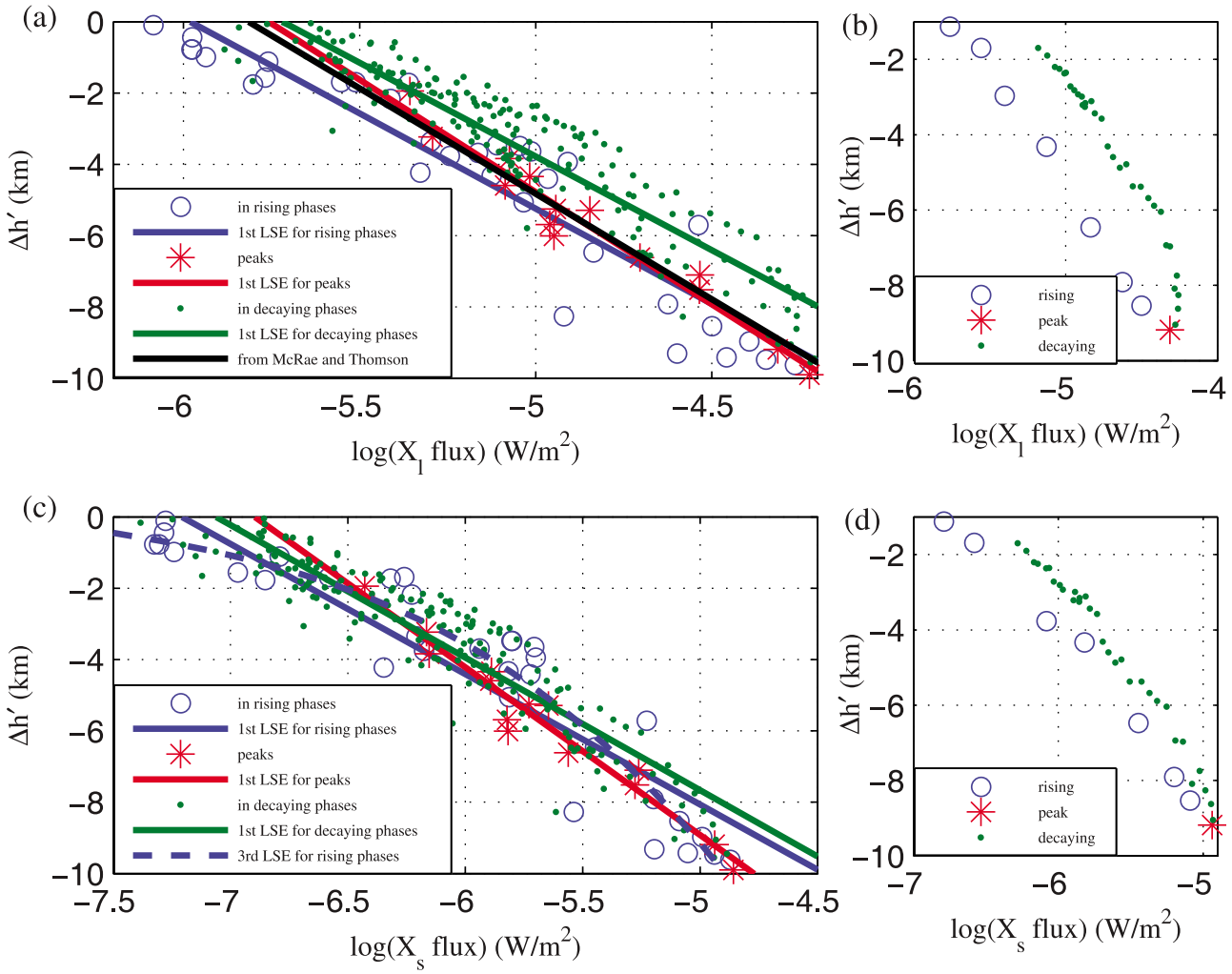

Figure 8. The measured $\Delta h'$ related to X-ray flux variation in two months. The $\Delta h'$ is approximately proportional to the logarithm of the X-ray fluxes. The same flux can induce different $\Delta h'$ in rising phases, peaks, and decaying phases of solar flares. (a) From 16 solar flare events for the long waveband. (b) From one solar flare event beginning at 10 LT on 13 July 2005 for the long waveband. (c) From 16 solar flare events for the short waveband. (d) From one solar flare event beginning at 10 LT on 13 July 2005 for the short waveband.

and $\Delta h'$ for 16 solar flare events. The first-order polynomial least square error (LSE) fit shows that an increase in flux by a factor of 10 (1 increase using logarithm) leads to 6.3 km decrease of h' in the X-ray peak time, which agrees perfectly with the results from narrowband measurements [*McRae and Thomson*, 2004]. This is also consistent with the results given by *Jacobson et al.* [2007], although the measured height has different meaning from h' here. However, when rising and decaying phase measurements are included, the relationship is more complex. The same X-ray flux increase leads to 5.4 km decrease of h' for both the rising and decaying phase. The solar flare has stronger effects on the D region in the rising phase than in the decaying phase, since the same flux can induce 1.5 km more h' decrease in the rising phase than in the decaying phase. This is also clearly shown in a single solar flare event. Figure 8b shows the comparison of $\Delta h'$ correlation with X_l fluxes in the rising and decaying phase for the solar flare beginning at 10 LT on 13 July 2005.

[38] Figure 8c shows the correlation between X_s fluxes and $\Delta h'$. An increase in flux by a factor of 10 leads to 4.7 km decrease of the h' in X-ray peak time but 3.7 km in both the rising and decaying phase. However, compared to the long waveband, the difference of the solar flare effects on D region during rising and decaying phases is much smaller. Only 0.5 km difference is generated by the same flux. This is also clearly shown by the solar flare event beginning at 10 LT on 13 July 2005 in Figure 8d. This indicates that h' changes correlate more consistently with the short, rather than the long wavelength X-ray fluxes.

[39] The 5 min average measurements in the rising phase as shown in Figure 8c exhibit a fairly clear nonlinear relationship between $\Delta h'$ and the logarithm of X_s fluxes. We applied the third order polynomial LSE fit to the correlation between the measured h' and X-ray fluxes in rising phases

of X_s. The same flux increase can lead to different h' decreases in different flux ranges. When the flux is small (logarithm smaller than −6.5), an increase in the flux by a factor of 10 only leads to h' decrease of 1.5 km. However, the same flux change can lead to 7.5 km h' decrease when the flux is large (logarithm larger than −5.5).

4. Summary and Conclusions

[40] In this work, we derived the midlatitude D region equivalent exponential electron density profile heights by comparing measured sferics to FDTD model simulated results. A total of 285,029 lightning strokes in July and August 2005 near Duke University provided almost continuous measurements during near 14 h daytime over a 2 month period.

[41] In daytime, as expected, the measured h' drops from sunrise to the lowest point at around noontime and resumes its ascending trend again. We found, on some days, the D region electron density profile height was also influenced by solar flare X-rays and the sudden drops form. They were observed in 9 days during 2 months.

[42] The correlation between 5 min average h' and the solar zenith angle on a certain day is similar to the result given by *McRae and Thomson* [2000], with the h' slightly higher in our measurements when the solar zenith angle is minimum. The rapid change of measured h' with solar zenith angle always showed up when the solar zenith angle was larger than 50 degrees. Based on the average measurements in 2 months, we found that, for the same solar zenith angle, especially when it was smaller than 70 degrees, our measured h' in local midlatitude regions is slightly higher than the polynomial calculation given by *McRae and Thomson* [2000] who measured the average h' in low-latitude long paths for near solar minimum years. The comparison of our results with a more complex model given by *Ferguson* [1980] also shows that only the general variation trend of h' with solar zenith angle is the same but the specific values of h' can show some differences.

[43] We also measured different regions simultaneously when the lightning locations were favorable. In order to exclude the solar zenith angle influence, we compared the measured h' in different geographic locations for the same solar zenith angle instead of local time. During 2 months, around half of the days exhibited regional differences not explained by the solar zenith angle. However, only 8 days had regional h' difference larger than 0.5 km when the solar zenith angle was the same. These results indicate that the ionospheric D region spatial variation beyond the solar zenith angle exists. The solar radiation is the dominant but not the only determinant source of the lower ionosphere ionization.

[44] Solar flare induced D region perturbations were studied in this work. Through comparing measured h' to X-ray fluxes recorded by GOES-10 satellite in 2 days, we found that those sudden drops in measured h' had good time correlations with the sudden increases of X-ray fluxes. Using 16 solar flare events during 2 months, we explored the quantitative relationship between X-ray fluxes and $\Delta h'$ in both the long waveband and short waveband in the X-ray rising phase, peak and decaying phase. The $\Delta h'$ is approximately proportional to the logarithm of X-ray fluxes. In the long waveband, an increase in the flux by a factor of 10 leads to 6.3 km decrease of h' in X-ray peak time, which agrees perfectly with the measurement given by *McRae and Thomson* [2004]. The same flux increase leads to 5.4 km decrease of h' in the X-ray rising and decaying phase. In the short waveband, the same flux increase leads to 4.7 km decrease of h' in X-ray peak time but 3.7 km in both the rising and decaying phase. Compared to the long waveband, the difference of the solar flare effects on D region during rising and decaying phases is much smaller in the short waveband. The measurement of h' shows that the relationship between $\Delta h'$ and X-ray flux for the rising phase in the short waveband is weakly nonlinear and we presented a third-order polynomial to describe this relationship.

[45] **Acknowledgments.** This research was supported by an NSF Aeronomy Program grant. We thank Gaopeng Lu and Jingbo Li for suggestions. The X-ray data were downloaded from http://spidr.ngdc.noaa.gov/spidr/.

[46] Philippa Browning thanks the reviewers for their assistance in evaluating this paper.

References

Balanis, C. A. (1989), *Advanced Engineering Electromagnetics*, 150 pp., John Wiley, New York.

Cheng, Z. (2006), Broadband VLF measurement of large/small scale D region ionospheric variabilities, Ph.D. thesis, Duke Univ., Durham, N. C.

Cheng, Z., S. A. Cummer, D. N. Baker, and S. G. Kanekal (2006), Nighttime *D* region electron density profiles and variabilities inferred from broadband measurements using VLF radio emissions from lightning, *J. Geophys. Res.*, *111*, A05302, doi:10.1029/2005JA011308.

Cummer, S. A. (2000), Modeling electromagnetic propagation in the Earth-ionosphere waveguide, *IEEE Trans. Antennas Propag.*, *48*(9), 1420–1429.

Cummer, S. A., U. S. Inan, and T. F. Bell (1998), Ionospheric *D* region remote sensing using VLF radio atmospherics, *Radio Sci.*, *33*, 1781–1792.

Cummins, K. L., E. P. Krider, and M. D. Malone (1998), The U. S. national lightning detection network and applications of cloud-to-ground lightning data by electric power utilities, *IEEE Trans. Electromagn. Compat.*, *40*(4), 465–480.

Deeks, D. G. (1966), D-region electron distributions in middle latitudes deduced from the reflection of long radio waves, *Proc. Soc. London*, *291*(10), 413–437.

Dennis, A. S., and E. T. Pierce (1967), The return stroke of the lightning flash to earth as a source of VLF atmospherics, *Radio Sci.*, *68D*, 777–794.

Ferguson, J. A. (1980), *Ionospheric profiles for predicting nighttime VLF/LF propagation*, *Naval Ocean Syst. Center Tech. Rep. 530*, Natl. Tech. Inf. Serv., Springfield. Va.

Friedrich, M., and K. M. Torkar (1983), Collision frequencies in the high-latitude D region, *J. Atmos. Terr. Phys.*, *45*, 267–271.

Goldberg, R. A., G. A. Lehmacher, F. J. Schmidlin, D. C. Fritts, J. D. Mitchell, C. L. Croskey, M. Friedrich, and W. E. Swartz (1997), Equatorial dynamics observed by rocket, radar, and satellite during the CADRE/MALTED campaign 1. Programmatics and small-scale fluctuations, *J. Geophys. Res.*, *102*(D22), 26,179–26,190, doi:10.1029/96JD03653.

Han, F., and S. A. Cummer (2010), Midlatitude nighttime D region ionosphere variability on hourly to monthly timescales, *J. Geophys. Res.*, *115*, A09323, doi:10.1029/2010JA015437.

Hu, W., and S. A. Cummer (2006), An FDTD model for low and high altitude lightning-generated EM fields, *IEEE Trans. Antennas Propag.*, *54*, 1513–1522.

Jacobson, A. R., R. Holzworth, E. Lay, M. Heavner, and D. A. Smith (2007), Low-frequency ionospheric sounding with narrow bipolar event lightning radio emissions: Regular variabilities and solar X-ray responses, *Ann. Geophys.*, *25*, 2175–2184.

Jacobson, A. R., X.-M. Shao, and R. Holzworth (2010), Full-wave reflection of lightning long-wave radio pulses from the ionospheric D region: Comparison with midday observations of broadband lightning signals, *J. Geophys. Res.*, *115*, A00E27, doi:10.1029/2009JA014540.

Jones, D. L. (1970), Electromagnetic radiation from multiple return strokes of lightning, *J. Atmos. Terr. Phys.*, *32*, 1077–1093.
Ma, Z., C. L. Croskeyb, and L. C. Haleb (1998), The electrodynamic responses of the atmosphere and ionosphere to the lightning discharge, *J. Atmos. Terr. Phys.*, *60*, 845–861.
McRae, W. M., and N. R. Thomson (2000), VLF phase and amplitude: Daytime ionospheric parameters, *J. Atmos. Terr. Phys.*, *62*, 609–618.
McRae, W. M., and N. R. Thomson (2004), Solar flare induced ionospheric D region enhancements from VLF phase and amplitude observations, *J. Atmos. Terr. Phys.*, *66*, 77–87.
Mechtly, E. A., and L. G. Smith (1968), Growth of the D region at sunrise, *J. Atmos. Terr. Phys.*, *30*, 363–369.
Mitra, A. P. (1974), *Ionospheric Effects of Solar Flares*, D. Reidel, Dordrecht, Netherlands.
Morfitt, D. G., and C. H. Shellman (1976), *MODESRCH: An Improved Computer Program for Obtaining ELF/VLF/LF Mode Constants in an Earth-Ionosphere Waveguide*, Nav. Electron Lab. Cent., San Diego, Calif.
Narcisi, R. S. (1971), Composition studies of the lower ionosphere, in *Physics of the Upper Atmosphere*, edited by F. Verniani, pp. 11–59, Editrice Compositori, Bologna, Italy.
Pant, P. (1993), Relation between VLF phase deviations and solar X-ray fluxes during solar flares, *Astrophys. Space Sci.*, *209*(2), 297–306.
Phelps, A. V., and J. L. Pack (1959), Electron collision frequencies in nitrogen and in the lower ionosphere, *Phys. Rev. Lett.*, *3*, 340–342.
Smith, D. A., M. J. Heavner, A. R. Jacobson, X. M. Shao, R. S. Massey, R. J. Sheldon, and K. C. Wiens (2004), A method for determining intracloud lightning and ionospheric heights from VLF/LF electric field records, *Radio Sci.*, *39*, RS1010, doi:10.1029/2002RS002790.
Smith, L. G., and B. E. Gilchrist (1984), Rocket observations of electron density in the nighttime E region using Faraday rotation, *Radio Sci.*, *19*(3), 913–924, doi:10.1029/RS019i003p00913.
Smith, L. G., and D. E. Klaus (1978), Rocket observations of electron density irregularities in the equatorial E region, *Space Res.*, *18*, 261–264.
Thomson, N. R. (1993), Experimental daytime VLF ionospheric parameters, *J. Atmos. Terr. Phys.*, *55*, 173–184.
Thomson, N. R., and M. A. Clilverd (2001), Solar flare induced ionospheric D region enhancements from VLF amplitude observations, *J. Atmos. Terr. Phys.*, *63*, 1729–1737.
Thomson, N. R., and W. M. McRae (2009), Nighttime ionospheric region: Equatorial and nonequatorial, *J. Geophys. Res.*, *114*, A08305, doi:10.1029/2008JA014001.
Thomson, N. R., C. J. Rodger, and R. L. Dowden (2004), Ionosphere gives size of greatest solar flare, *Geophys. Res. Lett.*, *31*, L06803, doi:10.1029/2003GL019345.
Thomson, N. R., C. J. Rodger, and M. A. Clilverd (2005), Large solar flares and their ionospheric D region enhancements, *J. Geophys. Res.*, *110*, A06306, doi:10.1029/2005JA011008.
Thomson, N. R., M. A. Clilverd, and W. M. McRae (2007), Nighttime D region parameters from VLF amplitude and phase, *J. Geophys. Res.*, *112*, A07304, doi:10.1029/2007JA012271.
Thrane, E. V., and W. R. Piggott (1966), The collision frequency in the E and D regions of the ionosphere, *J. Atmos. Terr. Phys.*, *28*, 721–737.
Todoroki, Y., S. Maekawa, T. Yamauchi, T. Horie, and M. Hayakawa (2007), Solar flare induced D region perturbation in the ionosphere, as revealed from a short-distance VLF propagation path, *Geophys. Res. Lett.*, *34*, L03103, doi:10.1029/2006GL028087.
Wait, J. R., and K. P. Spies (1964), *Characteristics of Earth-Ionosphere Waveguide for VLF Radio Waves*, Nat. Bur. of Stand., Boulder, Colo.

S. A. Cummer and F. Han, Department of Electrical and Computer Engineering, Duke University, Durham, NC 27708, USA. (cummer@ee.duke.edu; feng.han@duke.edu)